
Zero-Shot Uncertainty Quantification using Diffusion Probabilistic Models

Dule Shu

Department of Mechanical Engineering
Carnegie Mellon University
Pittsburgh, PA 15213
dules@andrew.cmu.edu

Amir Barati Farimani

Department of Mechanical Engineering
Carnegie Mellon University
Pittsburgh, PA 15213
barati@cmu.edu

Abstract

The success of diffusion probabilistic models in generative tasks, such as text-to-image generation, has motivated the exploration of their application to regression problems commonly encountered in scientific computing and various other domains. In this context, the use of diffusion regression models for ensemble prediction is becoming a practice with increasing popularity. Under such background, we conducted a study to quantitatively evaluate the effectiveness of ensemble methods on solving different regression problems using diffusion models. We consider the ensemble prediction of a diffusion model as a means for zero-shot uncertainty quantification, since the diffusion models in our study are not trained with a loss function containing any uncertainty estimation. Through extensive experiments on 1D and 2D data, we demonstrate that ensemble methods consistently improve model prediction accuracy across various regression tasks. Notably, we observed a larger accuracy gain in auto-regressive prediction compared with point-wise prediction, and that enhancements take place in both the mean-square error and the physics-informed loss. Additionally, we reveal a statistical correlation between ensemble prediction error and ensemble variance, offering insights into balancing computational complexity with prediction accuracy and monitoring prediction confidence in practical applications where the ground truth is unknown. Our study provides a comprehensive view of the utility of diffusion ensembles, serving as a useful reference for practitioners employing diffusion models in regression problem-solving.

1 Introduction

Ensemble learning [31] has long been used to improve the accuracy of prediction by combining multiple individual machine learning models. Applying ensemble learning to deep learning models has been an active area of research [2, 9, 12, 17, 23, 32, 53, 68], largely due to the success of deep learning in various application fields, with Deep Ensembles [32] being one of the representative works in this direction. Initially introduced as a simple and scalable method for estimating the predictive uncertainty of deep learning models, Deep Ensembles proposes to use a neural network architecture to predict both the mean and the variance of the target distribution, and formulates the training loss as the log-likelihood of a Gaussian distribution instead of the mean squared error of predictions. Deep Ensembles have been shown to enhance the model performance in terms of both prediction accuracy and uncertainty quantification in various applications [5, 35, 62, 63, 65, 66, 68]. Since its original formulation was introduced without a Bayesian inference form, Deep Ensembles was considered as an alternative and competing method to Bayesian neural networks [13, 47, 60] until the Bayesian formulation [23] of it is proposed using Bayesian model averaging [22]. In this work, we adopt the Bayesian formulation of Deep Ensembles and generalize this formulation to the diffusion ensembles, as further specified in Section 2.

The development of diffusion probabilistic models can be tracked to the method for learning a distribution inspired by Non-equilibrium Thermodynamics [56], and has gained a fast growth in popularity and technical advancement since their success on unconditional image generation tasks with the introduction of score network [58] and denoising diffusion probabilistic models (DDPM) [21]. The outstanding performance in generating imagery data motivates the exploration of using diffusion model as a regression model in tasks such as spatio-temporal data prediction [10, 14, 29, 34, 40, 45, 49, 51], super-resolution and inpainting [7, 33, 43, 55], bioinformatics [41, 67, 69], molecule property prediction [8, 15, 27], material property prediction [25, 48], optical flow estimation [44], image segmentation [1] and 3D feature reconstruction [24]. A key step of applying diffusion probabilistic models to solving regression problems is the incorporation of conditioning information to the backward diffusion process for data generation, since a regression model typically learns a mapping from a deterministic input to an deterministic output. In a diffusion probabilistic model, such mapping is often implemented as a conditional generation of the output given the input sample. Common methods to incorporate the conditioning information includes 1. Adding the gradient of the conditioning variable likelihood to the score function and 2. Using the conditioning variable to construct an intermediate state in solving the discretized stochastic differential equation. In either case, the computation of the denoising process (formulated as denoising score matching with Langevin Dynamics or ancestral sampling) iteratively inject a scaled Gaussian noise sample in model prediction (*e.g.*, z_i^M in Eq. 2, [59]), and the randomness of the noise sample results in the variability of model prediction. At a first glance, such variability might be undesirable to a regression task since the ground truth value of the prediction target is deterministic. However, it opens up the opportunity of using a diffusion regression model to generate a probabilistic output, which can be used for ensemble prediction and uncertainty quantification (UQ) [6, 11, 35, 46, 52, 65]. Unlike Deep Ensembles or popular UQ methods (*e.g.*, Quantile Regression [28, 50, 61], Mean Interval Score Regression [3, 65]) which incorporate an uncertainty metric into the model training loss, a diffusion probabilistic model does not require uncertainty estimation during model training, and allows the estimated variances of multiple prediction samples to be used as a natural choice of uncertainty metric. In this sense, we propose that a diffusion regression model is a natural tool for zero-shot uncertainty quantification.

In this work, we investigate the performance of diffusion regression models for ensemble learning and uncertainty quantification. An overview of our method for utilizing diffusion models in these contexts is presented in Fig. 1. To enhance the generalizability of our experimental results, we selected three diffusion models with different datasets and conditioning methods. Our experiments demonstrate that ensemble consistently reduces the model prediction error across a variety of regression tasks. Additionally, we observed a high correlation between prediction error and ensemble variance, indicating that diffusion ensemble serves as a simple tool for uncertainty quantification. The contribution of this work is summarized as follows.

1. We propose a Bayesian perspective of diffusion ensemble using BMA formulation.
2. We conduct an experiment of ensemble diffusion across different model designs and regression tasks. To the best of our knowledge, this is the first experiment of its kind to evaluate the effectiveness of ensemble on various regression diffusion models.
3. We show through numerical experiments that diffusion ensemble can serve as a convenient tool for uncertainty quantification, due to the high correlation between ensemble variance and the ensemble prediction accuracy.
4. We provide an analysis of the relationship between the ensemble variance and the ensemble size, offering a method to search for the appropriate ensemble size to balance computational complexity and gains in prediction accuracy.

2 Ensembled Prediction of Diffusion Model for Regression

We begin with reviewing the data generation process of denoising diffusion models and then propose our interpretation of its connection to Bayesian marginalization. In the score-based generative modeling [58], the following reverse-time stochastic differential equation (SDE) is proposed to model the data generation process.

$$dx = [f(x, t) - g(t)^2 \nabla_x \log p_t(x)] dt + g(t) dw, \quad (1)$$

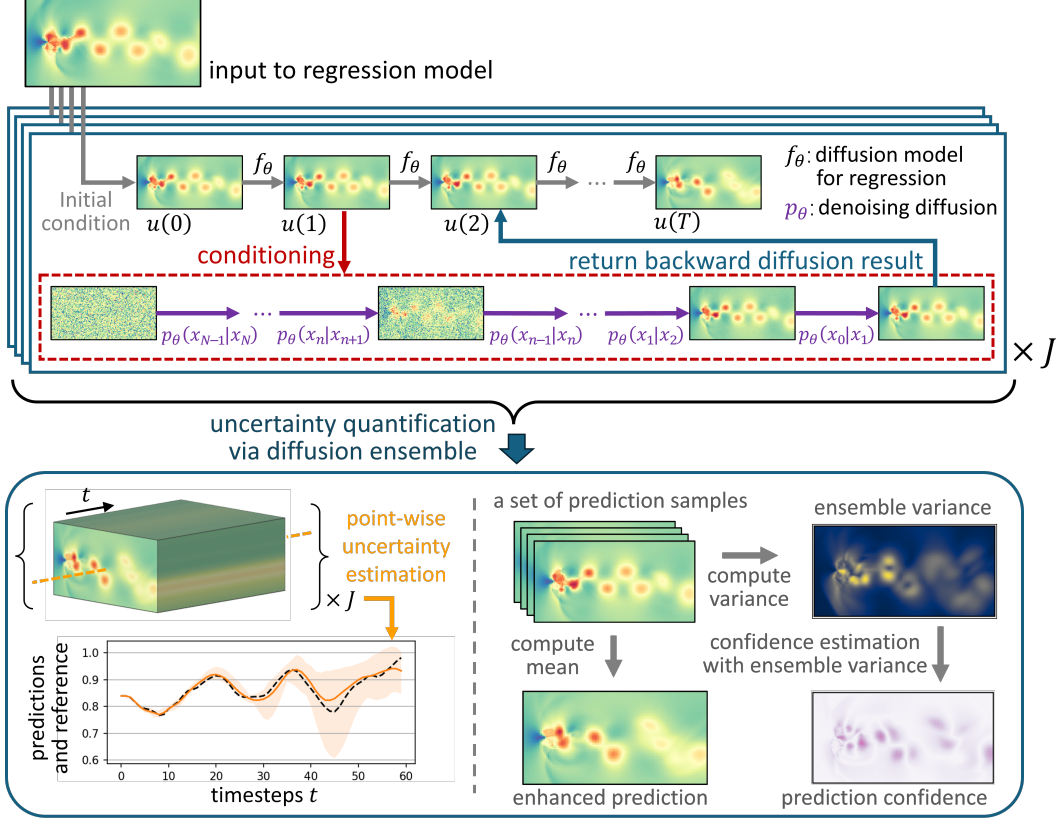


Figure 1: A overview of uncertainty quantification using diffusion probabilistic ensemble. With J ($J \geq 2$) samples of model prediction, we can estimate the prediction uncertainty at a given spatial location (lower-left plot), enhance the prediction accuracy via ensembled prediction (lower-middle plot), and use the ensemble variance to evaluate the prediction confidence (lower-right plot, where regions in dark purple color indicate a lower prediction confidence).

where $t \in [0, T]$ is the continuous time variable, $x(0) \sim p_0$ denotes a data sample, $x(T) \sim p_T$ denotes a noisy sample with a tractable prior distribution, f, g are the drift and diffusion coefficients, respectively (with respect to the forward diffusion process), w denotes a standard Wiener process, and $\nabla_x \log p_t(x)$ is the score of marginal distribution at time t . In practice, solving Eq. 1 to obtain $x(0)$ from $x(T)$ requires two conditions, 1. Using a neural network model $s_\theta(x, t)$ to estimate $\nabla_x \log p_t(x)$, and 2. Discretizing the time interval $[0, T]$ with an increasing sequence of time values $\{t_1, t_2, \dots, t_{N-1}\}$ and applying an iteration rule $x_i = h(x_{i+1})$ to obtain $x(0)$ from $x(T)$ (where $x_i := x(t_i)$, $x_0 := x(0)$ and $x_N := x(T)$). Two approaches are commonly used to achieve the second condition. The first approach, as used in DDPM sampling, computes a Markov chain $\prod_{i=1}^N p_\theta(x_{i-1}|x_i)$ with the following iteration rule:

$$x_i = h(x_{i+1}, s_\theta) := x_{i+1} + f_1 s_\theta(x_{i+1}, t_{i+1}) + f_2 z_{i+1}, \quad (2)$$

where f_1, f_2 are functions of noise scales, and $z_{i+1} \sim \mathcal{N}(\mathbf{0}, \mathbf{I})$. The second approach utilizes the result that for all diffusion processes modeled by an SDE, there exists a corresponding ordinary differential equation (ODE) whose trajectories share the same marginal probability densities as the SDE. Based on this derivation, the second approach either computes a deterministic iteration rule (excluding z_{i+1}) or employs a black-box ODE solver to solve for $x(0)$. However, Song *et al.* points out that samples obtained from directly solving the probability flow ODE typically have worse FID scores [58], and subsequently introduces a predictor-corrector iteration rule incorporating a Gaussian noise sample $z \sim \mathcal{N}(\mathbf{0}, \mathbf{I})$, which follows the same general form as shown in Eq. 2.

Wilson *et al.* [64] proposes the following formulation for the predictive distribution of Bayesian model averaging (BMA).

$$p(y|x, \mathcal{D}) = \int p(y|x, \mathbf{w})p(\mathbf{w}|\mathcal{D})d\mathbf{w},$$

where y denotes the output (*e.g.*, regression values), x denotes the input, \mathbf{w} denotes the weights of a neural network, and \mathcal{D} is the dataset. Considering the stochasticity of Eq. 2 which variates samples of a backward diffusion process conditioning on x , one can similarly derive a non-parametric BMA form of the backward diffusion process as follows.

$$p(x_0|x, \mathcal{D}) = \int p(x_0|x, x_1, x_2, \dots, x_N)p(x_1, x_2, \dots, x_N|\mathcal{D})d\mu(x_1, x_2, \dots, x_N), \quad (3)$$

where $x_0 \equiv y$ is the target variable of regression, and μ is a probability measure of random variables $\{x_i\}_{i=1}^N$. The BMA form of denoising diffusion model in Eq. 3 can be estimated with a simple Monte Carlo (MC) approximation as follows.

$$p(x_0|x, \mathcal{D}) \approx \frac{1}{J} \sum_{j=1}^J p(x_0|x, \mathbf{x}_{1:N}^{(j)}), \quad \mathbf{x}_{1:N}^{(j)} \sim p(\mathbf{x}_{1:N}|\mathcal{D}), \quad (4)$$

where $\mathbf{x}_{1:N}$ denotes the sequence of intermediate denoising states $\{x_i\}_{i=1}^N$, and $\mathbf{x}_{1:N}^{(j)}$ is the j th sample of $\mathbf{x}_{1:N}$. Eq. 4 specifies the formula for ensembled prediction of denoising diffusion models, which we refer to as diffusion ensemble in this paper.

3 Predictive Uncertainty Estimation of Diffusion Ensemble

We estimate the predictive uncertainty of a diffusion model for regression over a test dataset \mathcal{D} consisting of M data points, *e.g.*, $\mathcal{D} = \{x^{(m)}, y^{(m)}\}_{m=1}^M$. For regression problems, the label $y \in \{y^{(m)}\}_{m=1}^M$ is a real-valued variable sampled from a continuous space. Given an input data sample $x \in \{x^{(m)}\}_{m=1}^M$, we use a diffusion probabilistic model f_θ to compute the distribution of y , *e.g.*, $f_\theta(y|x)$. The predictive uncertainty of the model is measured by the mean and variance of prediction samples. Following the procedure to compute ensemble prediction specified in Eq. 4, for each input sample x , we compute J prediction samples, $\{\tilde{y}^{(j)}\}_{j=1}^J$, by recurrently sampling the Markov chain $\prod_{i=1}^N p_\theta(x_{i-1}|x_i)$ and assigning each sampled value of x_0 to $\tilde{y}^{(j)}$. Then, the mean of model prediction can be obtained as $\tilde{\mu}_y = \frac{1}{J} \sum_{j=1}^J \tilde{y}^{(j)}$. Since the label y is generally defined in a multi-dimensional real space (*e.g.*, $y \in \mathbb{R}^d$, $d \gg 1$), to provide a straightforward scalar quantification of the prediction variance, we take the mean of the point-wise prediction variance over all d dimensions as follows.

$$\bar{\sigma}^2(y) = \frac{1}{d} \sum_{k=1}^d \bar{\sigma}^2(\tilde{y}_k), \quad \bar{\sigma}^2(\tilde{y}_k) = \frac{1}{J-1} \sum_{j=1}^J \left(\tilde{y}_k^{(j)} - y_k \right)^2, \quad (5)$$

where the subscript k denotes the k th entry of the d -dimensional variables y and $\tilde{y} \in \{\tilde{y}^{(j)}\}_{j=1}^J$.

In uncertainty quantification literature, model predictive uncertainty is attributed to two types of uncertainty: aleatoric and epistemic. the aleatoric uncertainty and the epistemic uncertainty. Aleatoric uncertainty represents the intrinsic uncertainty of the prediction task and is therefore irreducible through model selection. In contrast, epistemic uncertainty represents the lack of knowledge of the model, which can be reduced by increasing the training data or improving the model. In the following section of Experiments, we show that the ensembled prediction defined by Eq. 4 helps reduce the prediction error attributed to the epistemic uncertainty in the regression tasks for the selected diffusion models. In general, reducing prediction error through ensemble requires that the ground truth of prediction target is sufficiently close to the mean of uncertainty estimate. In practice, users of a regression model can only assess whether their model meets this condition by testing the performance of ensemble on out-of-distribution data. A more detailed discussion on using uncertainty quantification to characterize and improve out-of-distribution learning can be found in [46]. Berry *et al.* [4] suggests that the epistemic uncertainty can be captured by the variance of sampled predictions of a deep ensemble model. With experimental results, we further demonstrate that the ensemble prediction variance is highly correlated with the prediction error. This observation,

while intuitive due to the connection between epistemic uncertainty and prediction error, indicates that denoising diffusion models are a class of low bias model for regression tasks. Moreover, one can potentially take advantage of such correlation by using the sampled variance as a metric to assess the reliability of a diffusion model’s prediction. Moreover, one can potentially leverage this correlation by using the sampled variance as a metric to assess the reliability of a diffusion model’s prediction, which can be particularly helpful in practical applications where ground truth labels are unknown. Admittedly, the benefits of ensemble prediction come at the cost of increased computational complexity. Therefore, we conducted numerical experiments to show the convergence rate of the Monte Carlo (MC) approximations defined by Equations 4 and 5, providing a quantified evaluation of the computational cost of ensemble prediction.

4 Experiments

In this section, we show the results of ensembled learning on three different diffusion models for regression, PDE-Refiner [40], ACDM [30], and a physics-informed diffusion model for fluid flow super-resolution [55] (which we referred to as PI-DFS for simplicity). All three models are developed as surrogate models for simulating physical processes governed by partial differential equations. For each model, we sample multiple predictions of the target quantity of interest, compute the ensembled prediction as the estimated means by MC approximation, and compare the prediction error of the ensembled prediction and all sampled predictions. To evaluate the variance of prediction, we compute the point-wise estimated variance of the prediction samples at each location of the data domain, visualize the variance at selected locations and simulation runs, and compute the correlation between averaged variance and prediction error over simulation timesteps. In addition, we varies the value of J from Equations 4 and 5 to show the rate of convergence of MC approximation.

4.1 PDE-Refiner

PDE-Refiner is a model designed to produce more accurate and stable predictions of time-dependent PDE solutions. To achieve this goal, the model learns to refine an initial prediction by applying a backward diffusion process conditioned on that initial condition. The authors suggest that the refinement process in a diffusion style helps to preserve non-dominant high spatial frequency information in PDE solutions and therefore reduces the prediction error in long time rollout (autoregressive prediction) in their numerical experiments. More specifically, given a PDE solution at a previous timestep, $u(t - \Delta t)$, PDE-Refiner uses a neural operator model f_θ to make an initial prediction of the PDE solution at the current step, *e.g.*, $\hat{u}^0(t) = f_\theta(u(t - \Delta t))$. Next, a K -step iterative refinement process is applied to the initial prediction to obtain a refined prediction as follows.

$$\begin{aligned} \hat{z} &= f_\theta(\hat{u}^{k-1}(t) + \sigma_k z; u(t - \Delta t), k), \\ \hat{u}^k(t) &= \hat{u}^{k-1}(t) + \sigma_k z - \sigma_k \hat{z}, \quad k \in \{1, 2, \dots, K\}, \end{aligned}$$

where σ_k denotes the noise scale, and $z \sim \mathcal{N}(\mathbf{0}, \mathbf{I})$. While the network architecture for f_θ is chosen as a U-Net [16], the refine-by-denoising idea of PDE-Refiner is applicable to other network architectures such as the popular Transformer family of neural PDE solvers [18, 19, 36–38, 42, 54, 70, 71].

4.2 ACDM

Similar to PDE-Refiner, the Autoregressive Conditional Diffusion Model (ACDM) is another model for simulating turbulent flows where diffusion processes are used to enhance the temporal stability of long rollouts. Unlike PDE-Refiner, ACDM computes a complete backward diffusion process starting from noise samples to predict the physical quantity of interest at the next timestep, where the values of the physical quantity at the current timestep and other PDE-related information are incorporated via forward process into every denoising step. ACDM outperforms PDE-Refiner on benchmark experiments at a cost of lower inference speed [30]. Let $u(t)$ denote the physical quantity of interest evaluated at timesteps t , and let c_f be the set of coefficients related to the PDE model of the simulation (*e.g.*, Reynolds number or Mach number for fluid dynamics simulation). ACDM predicts $u(t)$, a state variable at current timestep, using the previous k steps of the states, $\{u(t-1), u(t-2), \dots, u(t-k)\}$ and the coefficients c_f . A basic DDPM algorithm is used to compute an R -step backward diffusion process starting from $x_R := (d_R, c_R)$ and ending at $x_0 = (d_0, c_0)$, where $d_R \sim \mathcal{N}(\mathbf{0}, \mathbf{I})$, $c_0 = \{u(t-1), u(t-2), \dots, u(t-k), c_f\}$, $\{c_r\}_{r=1}^R$ is obtained from c_0 via

reparameterization, the state transition is computed by a neural network via $x_{r-1} \sim p_\theta(x_{r-1}|x_r)$, and d_0 is the final prediction of the target $u(t)$.

4.3 PI-DFS

To evaluate the effectiveness of ensembled prediction on a wider range of regression problems for a diffusion model, we include experimental results with the PI-DFS model. PI-DFS model is chosen because it differs from PDE-Refiner and ACDM on two key aspects. 1. Unlike PDE-Refiner or ACDM, which are used for auto-regressive prediction of time-series data given an initial condition, PI-DFS is employed for making point-wise predictions from input to output. 2. PI-DFS is designed to minimize not only the point-wise prediction error (*e.g.*, the \mathcal{L}^2 distance between the prediction and the ground truth) but also the physics-informed loss defined as the PDE residual of model predictions. Let u_l, u_h be a low fidelity and a high fidelity data samples of some physical quantity of interest (*e.g.*, the vorticity of fluid evaluated on a 2D mesh). In model inference stage, the PI-DFS model takes u_l as input and predicts the value of u_h . To achieve this goal, PI-DFS first uses u_l to construct an estimated intermediate state of a backward diffusion process for predicting u_h as follows.

$$x_\tau := \sqrt{\bar{\alpha}_\tau} u_l + \sqrt{1 - \bar{\alpha}_\tau} \epsilon_\tau,$$

where $\epsilon_\tau \sim \mathcal{N}(\mathbf{0}, \mathbf{I})$, and $\bar{\alpha}_\tau$ is a noise scheduling parameter at denoising timestep τ following the notation in [21]. Then, a denoising diffusion implicit model (DDIM) [57] starting from x_τ is computed to obtain x_0 , the final state of the reverse process, as a prediction of u_h . At each step of denoising, the corresponding state variable, denoted as x_{τ_i} , is substituted into the governing PDE (*e.g.*, a 2D Navier-Stokes equation) to compute the residual. The relative \mathcal{L}^2 norm of the residual, defined as the physics-informed residual loss, is used as classifier-free guidance [20] to guide the data generation process for a minimized residual loss.

4.4 Common observations from listed tasks

In this subsection, we summarize the phenomena commonly observed in the three numerical experiments using different diffusion models presented above. This serves to analyze the general properties of diffusion models used as a deep ensemble model for regression problems. Our observations are as follows. 1. Ensemble improves the accuracy of model predictions. 2. The accuracy of ensembled prediction is highly correlated with the variance of the prediction samples. Further comments and quantitative evaluations regarding these two observations are presented as follows.

Table 1: A comparison of accuracy between sampled predictions and ensemble predictions, where the accuracy is evaluated by the relative \mathcal{L}^2 error for all models and by the PDE residual loss for the PI-DFS model. For the tasks of auto-regressive predictions, the prediction error is evaluated at the final time-step. For the task of point-wise prediction, the metrics are evaluated across initial conditions and timesteps of the reference simulation data used as the test dataset.

model	prediction error		residual loss		Task description
	sampled mean	ensemble	sampled mean	ensemble	
PDE-Refiner	0.1192	0.0986	—	—	Auto-regressive prediction on 1D data.
ACDM	0.5516	0.3966	—	—	Auto-regressive prediction on 2D data with 4 data channels.
PI-DFS	0.3752	0.3657	0.2586	0.1846	Point-wise prediction on 2D data.

Improvements on prediction accuracy. The improvements on prediction accuracy across different regression tasks are shown in Figures 4a, 5a, 6, and Table 1. Among the three tasks evaluated in

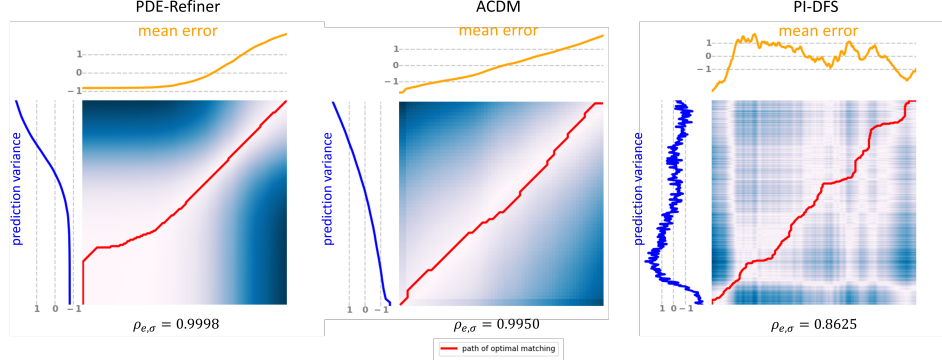


Figure 2: Dynamic Time Warping similarity between the spatial means of ensemble prediction variance and ensemble prediction error, where the Euclidean distance is used as the distance metric and the color map (varying from white to blue) for coloring the background.

this paper, auto-regressive prediction gains a larger accuracy increase than point-wise prediction (by which we mean the model inputs are always sampled from test datasets rather than from its own outputs) in terms of the relative \mathcal{L}^2 error. This observation implies that ensemble is an effective strategy for countering the accumulative error in auto-regression. The experimental results with PI-DFS demonstrate that ensemble is capable of reducing both the \mathcal{L}^p loss and the physics-informed loss. Note that both losses are computed by averaging the corresponding metric function (*e.g.*, the \mathcal{L}^p distance and the PDE residual) over the spatial domain of interest. In comparison, accuracy improvement by ensemble is not observed in statistical metrics such as the kinetic energy spectrum and the vorticity distribution. It would be interesting to see whether ensemble can also improve the frequency domain accuracy metrics of model predictions such as the kinetic energy spectrum by applying to frequency-domain features (*e.g.*, the Fourier coefficient features obtained from Fast Fourier Transform as proposed in [39]) in model forward propagation.

Correlations between prediction variance and accuracy. Throughout the regression tasks solved with different diffusion models in our study, we have observed a consistent correlation between the variance of the ensemble and its prediction accuracy. Specifically, it is observed that the relative \mathcal{L}^2 prediction error $e(t)$, defined by Eq. 6, is highly correlated with the ensemble variance defined as follows.

$$\sigma_u^2(t) = \frac{1}{B \cdot D \cdot C} \sum_{b=1}^B \sum_{d=1}^D \sum_{c=1}^C \sigma_u^2(b, t, d, c)$$

where $\sigma_u^2(b, t, d, c) = \frac{1}{16} \sum_{j=1}^{16} \left(\tilde{u}^{(j)}(b, t, d, c) - \mu_u(b, t, d, c) \right)^2$.

Figure 2 shows the values of Pearson correlation coefficient (denoted as $\rho_{e, \sigma}$) as a way to evaluate the correlation between the time sequences $\{e(t)\}_{t=1}^T$ and $\{\sigma_u^2(t)\}_{t=1}^T$ in different tasks. Also shown in the figure are the Dynamic Time Warping (DTW) similarity between $\{e(t)\}_{t=1}^T$ and $\{\sigma_u^2(t)\}_{t=1}^T$. The results that $\rho_{e, \sigma}$ has a value close to 1 and that the optimal matching paths (marked by red solid lines) are close to the diagonal line demonstrate the high correlation between the ensemble variance and the ensemble prediction error. With such correlation, users of a diffusion model can compute the ensemble variance to assess the accuracy and reliability of the model prediction in a practical application scenario where the ground truth reference is unknown and the knowledge of the model prediction error are unavailable.

The advantage of using a diffusion model for ensembled prediction, including improvements on prediction accuracy and the utility of assessing prediction accuracy, come at a cost of increased computational complexity. To provide a quantified analysis on the trade-off between the benefit of ensemble and its computational cost, we propose the following method to examine how the ensemble variance (which are highly correlated to the prediction accuracy, as shown in Fig. 2) changes with respect to the ensemble size. Let $\{\tilde{u}^{(j)}\}_{j=1}^N$ be N prediction samples collected for a maximal ensemble size, and let $k \in \{2, 3, \dots, N\}$ be a chosen size of an ensembled prediction. For each

k -combination of the N samples represented by the corresponding index set $\mathcal{J}_k^{(m)}$, we compute the point-wise standard deviation of the k samples as follows.

$$\sigma_k^{(m)}(b, t, d, c) = \left(\frac{1}{k} \sum_{j \in \mathcal{J}_k^{(m)}} \left(\tilde{u}^{(j)}(b, t, d, c) - \mu_k^{(m)}(b, t, d, c) \right)^2 \right)^{\frac{1}{2}}$$

where $\mu_k^{(m)}(b, t, d, c) = \frac{1}{k} \sum_{j \in \mathcal{J}_k^{(m)}} \tilde{u}^{(j)}(b, t, d, c).$

Then, we compute the mean of $\sigma_k^{(m)}(b, t, d, c)$ over all data dimensions (e.g., $[1, B] \times [1, T] \times [1, D] \times [1, C]$), denoted as $\bar{\sigma}_k^{(m)}$, as a scalar metric to quantify the ensemble variance for the sample index set $\mathcal{J}_k^{(m)}$. For each ensemble size k , we obtain a set of ensemble variance values using our proposed metric, e.g., $\{\bar{\sigma}_k^{(1)}, \bar{\sigma}_k^{(2)}, \dots, \bar{\sigma}_k^{(M)}\}$ where $M = C_k^N$. By plotting the values in the set and their

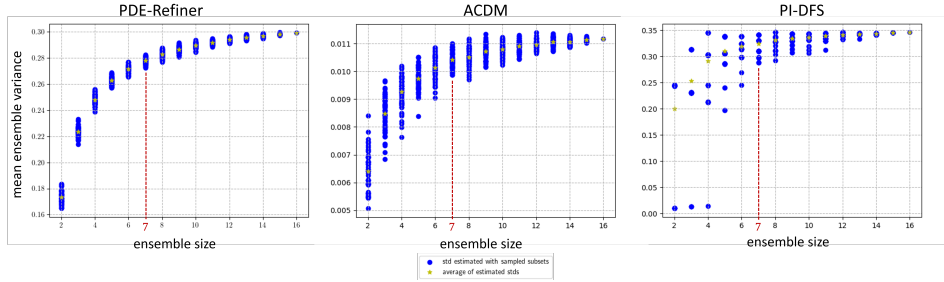


Figure 3: The plots of mean ensemble variances for different ensemble sizes. The ensemble size are chosen as 7 by observing the convergence of the mean variance with respect to the increase of ensemble size to balance the benefit of ensemble and its computational complexity.

mean for all ensemble sizes $2 \leq k \leq N$, we can visualize how the ensemble variance converges with respect to the ensemble size, and choose a proper ensemble size for a reduced computational cost. Figure 3 shows the plot of mean ensemble variances for different ensemble sizes. In all three tasks, a pattern of convergence of the mean ensemble variance can be observed as the ensemble size increases. As an example, we empirically choose $k = 7$ by observing the plots to balance the gain of ensemble prediction with its computational complexity. With a different diffusion model, the user can adopt the same procedure to determine the size of ensemble.

5 Conclusion

In this work, we investigate the effect of ensemble prediction on diffusion models for regression tasks. We start with a Bayesian formulation of the ensemble prediction by incorporating the backward diffusion process into a BMA framework, then propose to use the spatial mean of point-wise ensemble variance as a metric to quantify the predictive uncertainty estimation. Numerical experiments on three different regression tasks demonstrate the effectiveness of ensemble methods on diffusion probabilistic models. Our results show that ensemble consistently improve the prediction accuracy of diffusion models, albeit to varying degrees across different tasks. Additionally, we observe a high correlation between ensemble prediction error and mean ensemble variance, indicating that diffusion ensembles provide a straightforward and convenient tool for uncertainty quantification without requiring specialized model training procedures to minimize a predefined uncertainty quantification metric. Our future work will focus on further exploring the correlation between ensemble error and variance. A promising direction is uncertainty-based importance sampling for data-efficient fine-tuning of diffusion regression models. Specifically, by modifying the model training procedure as proposed by Katharopoulos *et al.* [26], the mean ensemble variance can be computed as an importance score for weighted data sampling. This approach ensures that input data samples leading to higher prediction uncertainty (and consequently higher prediction error) are more likely to be selected for querying the ground truth label, thereby minimizing data usage for model fine-tuning.

6 Acknowledgement

This work is supported by funding from the Division of Chemical, Bioengineering, Environmental and Transport Systems at National Science Foundation (CBET-1953222), United States. The authors would also like to thank Hongshuo Huang for helping with data sampling and Zijie Li for the inspiring discussions on problem formulation and references.

References

- [1] Tomer Amit, Tal Shaharbany, Eliya Nachmani, and Lior Wolf. Segdiff: Image segmentation with diffusion probabilistic models. *arXiv preprint arXiv:2112.00390*, 2021.
- [2] Devansh Arpit, Huan Wang, Yingbo Zhou, and Caiming Xiong. Ensemble of averages: Improving model selection and boosting performance in domain generalization. *Advances in Neural Information Processing Systems*, 35:8265–8277, 2022.
- [3] Ross Askanazi, Francis X Diebold, Frank Schorfheide, and Minchul Shin. On the comparison of interval forecasts. *Journal of Time Series Analysis*, 39(6):953–965, 2018.
- [4] Lucas Berry, Axel Brando, and David Meger. Casting light on large generative networks: Taming epistemic uncertainty in diffusion models. 2024. URL <https://openreview.net/forum?id=HqQctXKI7W>.
- [5] Yue Cao, Thomas Andrew Geddes, Jean Yee Hwa Yang, and Pengyi Yang. Ensemble deep learning in bioinformatics. *Nature Machine Intelligence*, 2(9):500–508, 2020.
- [6] Matthew A Chan, Maria J Molina, and Christopher A Metzler. Hyper-diffusion: Estimating epistemic and aleatoric uncertainty with a single model. *arXiv preprint arXiv:2402.03478*, 2024.
- [7] Runmin Dong, Shuai Yuan, Bin Luo, Mengxuan Chen, Jinxiao Zhang, Lixian Zhang, Weijia Li, Juepeng Zheng, and Haohuan Fu. Building bridges across spatial and temporal resolutions: Reference-based super-resolution via change priors and conditional diffusion model. In *Proceedings of the IEEE/CVF Conference on Computer Vision and Pattern Recognition*, pages 27684–27694, 2024.
- [8] Yiqun Duan, Xianda Guo, and Zheng Zhu. Diffusiondepth: Diffusion denoising approach for monocular depth estimation. *arXiv preprint arXiv:2303.05021*, 2023.
- [9] Yousef El-Laham, Niccolò Dalmaso, Elizabeth Fons, and Svitlana Vyetrenko. Deep gaussian mixture ensembles. In *Uncertainty in Artificial Intelligence*, pages 549–559. PMLR, 2023.
- [10] Runyang Feng, Yixing Gao, Tze Ho Elden Tse, Xueqing Ma, and Hyung Jin Chang. Diffpose: Spatiotemporal diffusion model for video-based human pose estimation. In *Proceedings of the IEEE/CVF International Conference on Computer Vision*, pages 14861–14872, 2023.
- [11] Marc Anton Finzi, Anudhyan Boral, Andrew Gordon Wilson, Fei Sha, and Leonardo Zepeda-Núñez. User-defined event sampling and uncertainty quantification in diffusion models for physical dynamical systems. In *International Conference on Machine Learning*, pages 10136–10152. PMLR, 2023.
- [12] Stanislav Fort, Huiyi Hu, and Balaji Lakshminarayanan. Deep ensembles: A loss landscape perspective. *arXiv preprint arXiv:1912.02757*, 2019.
- [13] Gianni Franchi, Andrei Bursuc, Emanuel Aldea, Séverine Dubuisson, and Isabelle Bloch. Encoding the latent posterior of bayesian neural networks for uncertainty quantification. *IEEE Transactions on Pattern Analysis and Machine Intelligence*, 2023.
- [14] Han Gao, Xu Han, Xiantao Fan, Luning Sun, Li-Ping Liu, Lian Duan, and Jian-Xun Wang. Bayesian conditional diffusion models for versatile spatiotemporal turbulence generation. *Computer Methods in Applied Mechanics and Engineering*, 427:117023, 2024.

- [15] Jiaqi Guan, Wesley Wei Qian, Xingang Peng, Yufeng Su, Jian Peng, and Jianzhu Ma. 3d equivariant diffusion for target-aware molecule generation and affinity prediction. *arXiv preprint arXiv:2303.03543*, 2023.
- [16] Jayesh K Gupta and Johannes Brandstetter. Towards multi-spatiotemporal-scale generalized pde modeling. *arXiv preprint arXiv:2209.15616*, 2022.
- [17] Bobby He, Balaji Lakshminarayanan, and Yee Whye Teh. Bayesian deep ensembles via the neural tangent kernel. *Advances in neural information processing systems*, 33:1010–1022, 2020.
- [18] AmirPouya Hemmasian and Amir Barati Farimani. Multi-scale time-stepping of partial differential equations with transformers. *Computer Methods in Applied Mechanics and Engineering*, 426:116983, 2024.
- [19] AmirPouya Hemmasian and Amir Barati Farimani. Pretraining a neural operator in lower dimensions. *arXiv preprint arXiv:2407.17616*, 2024.
- [20] Jonathan Ho and Tim Salimans. Classifier-free diffusion guidance. *arXiv preprint arXiv:2207.12598*, 2022.
- [21] Jonathan Ho, Ajay Jain, and Pieter Abbeel. Denoising diffusion probabilistic models. *Advances in neural information processing systems*, 33:6840–6851, 2020.
- [22] Jennifer A Hoeting, David Madigan, Adrian E Raftery, and Chris T Volinsky. Bayesian model averaging: a tutorial (with comments by m. clyde, david draper and ei george, and a rejoinder by the authors. *Statistical science*, 14(4):382–417, 1999.
- [23] Lara Hoffmann and Clemens Elster. Deep ensembles from a bayesian perspective. *arXiv preprint arXiv:2105.13283*, 2021.
- [24] Maksym Ivashechkin, Oscar Mendez, and Richard Bowden. Denoising diffusion for 3d hand pose estimation from images. In *Proceedings of the IEEE/CVF International Conference on Computer Vision*, pages 3136–3145, 2023.
- [25] Yayati Jadhav, Joseph Berthel, Chunshan Hu, Rahul Panat, Jack Beuth, and Amir Barati Farimani. Stressd: 2d stress estimation using denoising diffusion model. *Computer Methods in Applied Mechanics and Engineering*, 416:116343, 2023.
- [26] Angelos Katharopoulos and François Fleuret. Not all samples are created equal: Deep learning with importance sampling. In *International conference on machine learning*, pages 2525–2534. PMLR, 2018.
- [27] Seonghwan Kim, Jeheon Woo, and Woo Youn Kim. Diffusion-based generative ai for exploring transition states from 2d molecular graphs. *Nature Communications*, 15(1):341, 2024.
- [28] Danijel Kivaranovic, Kory D Johnson, and Hannes Leeb. Adaptive, distribution-free prediction intervals for deep networks. In *International Conference on Artificial Intelligence and Statistics*, pages 4346–4356. PMLR, 2020.
- [29] Georg Kohl, Li-Wei Chen, and Nils Thuerey. Turbulent flow simulation using autoregressive conditional diffusion models. *arXiv preprint arXiv:2309.01745*, 2023.
- [30] Georg Kohl, Li-Wei Chen, and Nils Thuerey. Benchmarking autoregressive conditional diffusion models for turbulent flow simulation, 2024. URL <https://arxiv.org/abs/2309.01745>.
- [31] Gautam Kunapuli. *Ensemble methods for machine learning*. Simon and Schuster, 2023.
- [32] Balaji Lakshminarayanan, Alexander Pritzel, and Charles Blundell. Simple and scalable predictive uncertainty estimation using deep ensembles. *Advances in neural information processing systems*, 30, 2017.
- [33] Charles Laroche, Andrés Almansa, and Eva Coupete. Fast diffusion em: a diffusion model for blind inverse problems with application to deconvolution. In *Proceedings of the IEEE/CVF Winter Conference on Applications of Computer Vision*, pages 5271–5281, 2024.

- [34] Lizao Li, Rob Carver, Ignacio Lopez-Gomez, Fei Sha, and John Anderson. Seeds: Emulation of weather forecast ensembles with diffusion models. *arXiv preprint arXiv:2306.14066*, 2023.
- [35] Longze Li, Jiang Chang, Aleksandar Vakanski, Yachun Wang, Tiankai Yao, and Min Xian. Uncertainty quantification in multivariable regression for material property prediction with bayesian neural networks. *Scientific Reports*, 14(1):10543, 2024.
- [36] Zijie Li, Kazem Meidani, and Amir Barati Farimani. Transformer for partial differential equations’ operator learning. *arXiv preprint arXiv:2205.13671*, 2022.
- [37] Zijie Li, Dule Shu, and Amir Barati Farimani. Scalable transformer for pde surrogate modeling. *Advances in Neural Information Processing Systems*, 36, 2024.
- [38] Zijie Li, Anthony Zhou, Saurabh Patil, and Amir Barati Farimani. Cafa: Global weather forecasting with factorized attention on sphere. *arXiv preprint arXiv:2405.07395*, 2024.
- [39] Zongyi Li, Nikola Borislavov Kovachki, Kamyar Azizzadenesheli, Burigede liu, Kaushik Bhattacharya, Andrew Stuart, and Anima Anandkumar. Fourier neural operator for parametric partial differential equations. In *International Conference on Learning Representations*, 2021. URL <https://openreview.net/forum?id=c8P9NQVtmn0>.
- [40] Phillip Lippe, Bas Veeling, Paris Perdikaris, Richard Turner, and Johannes Brandstetter. Pde-refiner: Achieving accurate long rollouts with neural pde solvers. *Advances in Neural Information Processing Systems*, 36, 2024.
- [41] Shiwei Liu, Tian Zhu, Milong Ren, Chungong Yu, Dongbo Bu, and Haicang Zhang. Predicting mutational effects on protein-protein binding via a side-chain diffusion probabilistic model. *Advances in Neural Information Processing Systems*, 36, 2024.
- [42] Cooper Lorsung, Zijie Li, and Amir Barati Farimani. Physics informed token transformer for solving partial differential equations. *Machine Learning: Science and Technology*, 5(1):015032, 2024.
- [43] Andreas Lugmayr, Martin Danelljan, Andres Romero, Fisher Yu, Radu Timofte, and Luc Van Gool. Repaint: Inpainting using denoising diffusion probabilistic models. In *Proceedings of the IEEE/CVF conference on computer vision and pattern recognition*, pages 11461–11471, 2022.
- [44] Ao Luo, Xin Li, Fan Yang, Jiangyu Liu, Haoqiang Fan, and Shuaicheng Liu. Flowdiffuser: Advancing optical flow estimation with diffusion models. In *Proceedings of the IEEE/CVF Conference on Computer Vision and Pattern Recognition*, pages 19167–19176, 2024.
- [45] Weibo Mao, Chenxin Xu, Qi Zhu, Siheng Chen, and Yanfeng Wang. Leapfrog diffusion model for stochastic trajectory prediction. In *Proceedings of the IEEE/CVF conference on computer vision and pattern recognition*, pages 5517–5526, 2023.
- [46] S Chandra Mouli, Danielle C Maddix, Shima Alizadeh, Gaurav Gupta, Andrew Stuart, Michael W Mahoney, and Yuyang Wang. Using uncertainty quantification to characterize and improve out-of-domain learning for pdes. *arXiv preprint arXiv:2403.10642*, 2024.
- [47] Radford M Neal. *Bayesian learning for neural networks*, volume 118. Springer Science & Business Media, 2012.
- [48] Francis Ogoke, Quanliang Liu, Olabode Ajenifujah, Alexander Myers, Guadalupe Quirarte, Jonathan Malen, Jack Beuth, and Amir Barati Farimani. Inexpensive high fidelity melt pool models in additive manufacturing using generative deep diffusion. *Materials & Design*, page 113181, 2024.
- [49] Oded Ovadia, Eli Turkel, Adar Kahana, and George Em Karniadakis. Ditto: Diffusion-inspired temporal transformer operator. *arXiv preprint arXiv:2307.09072*, 2023.
- [50] Tim Pearce, Alexandra Brintrup, Mohamed Zaki, and Andy Neely. High-quality prediction intervals for deep learning: A distribution-free, ensembled approach. In *International conference on machine learning*, pages 4075–4084. PMLR, 2018.

- [51] Ilan Price, Alvaro Sanchez-Gonzalez, Ferran Alet, Timo Ewalds, Andrew El-Kadi, Jacklynn Stott, Shakir Mohamed, Peter Battaglia, Remi Lam, and Matthew Willson. Gencast: Diffusion-based ensemble forecasting for medium-range weather. *arXiv preprint arXiv:2312.15796*, 2023.
- [52] Rahul Rahaman et al. Uncertainty quantification and deep ensembles. *Advances in neural information processing systems*, 34:20063–20075, 2021.
- [53] Florian Seligmann, Philipp Becker, Michael Volpp, and Gerhard Neumann. Beyond deep ensembles: A large-scale evaluation of bayesian deep learning under distribution shift. *Advances in Neural Information Processing Systems*, 36, 2024.
- [54] Benjamin Shih, Ahmad Peyvan, Zhongqiang Zhang, and George Em Karniadakis. Transformers as neural operators for solutions of differential equations with finite regularity. *arXiv preprint arXiv:2405.19166*, 2024.
- [55] Dule Shu, Zijie Li, and Amir Barati Farimani. A physics-informed diffusion model for high-fidelity flow field reconstruction. *Journal of Computational Physics*, 478:111972, 2023.
- [56] Jascha Sohl-Dickstein, Eric Weiss, Niru Maheswaranathan, and Surya Ganguli. Deep unsupervised learning using nonequilibrium thermodynamics. In *International conference on machine learning*, pages 2256–2265. PMLR, 2015.
- [57] Jiaming Song, Chenlin Meng, and Stefano Ermon. Denoising diffusion implicit models. *arXiv preprint arXiv:2010.02502*, 2020.
- [58] Yang Song and Stefano Ermon. Generative modeling by estimating gradients of the data distribution. *Advances in neural information processing systems*, 32, 2019.
- [59] Yang Song, Jascha Narain Sohl-Dickstein, Diederik P. Kingma, Abhishek Kumar, Stefano Ermon, and Ben Poole. Score-based generative modeling through stochastic differential equations. *ArXiv*, abs/2011.13456, 2020. URL <https://api.semanticscholar.org/CorpusID:227209335>.
- [60] Luning Sun and Jian-Xun Wang. Physics-constrained bayesian neural network for fluid flow reconstruction with sparse and noisy data. *Theoretical and Applied Mechanics Letters*, 10(3): 161–169, 2020.
- [61] Natasa Tagasovska and David Lopez-Paz. Single-model uncertainties for deep learning. *Advances in neural information processing systems*, 32, 2019.
- [62] Abdul Wasay, Brian Hentschel, Yuze Liao, Sanyuan Chen, and Stratos Idreos. Mothernets: Rapid deep ensemble learning. *Proceedings of Machine Learning and Systems*, 2:199–215, 2020.
- [63] Florian Wenzel, Jasper Snoek, Dustin Tran, and Rodolphe Jenatton. Hyperparameter ensembles for robustness and uncertainty quantification. *Advances in Neural Information Processing Systems*, 33:6514–6527, 2020.
- [64] Andrew G Wilson and Pavel Izmailov. Bayesian deep learning and a probabilistic perspective of generalization. *Advances in neural information processing systems*, 33:4697–4708, 2020.
- [65] Dongxia Wu, Liyao Gao, Matteo Chinazzi, Xinyue Xiong, Alessandro Vespignani, Yi-An Ma, and Rose Yu. Quantifying uncertainty in deep spatiotemporal forecasting. In *Proceedings of the 27th ACM SIGKDD Conference on Knowledge Discovery & Data Mining*, pages 1841–1851, 2021.
- [66] Yongquan Yang, Haijun Lv, and Ning Chen. A survey on ensemble learning under the era of deep learning. *Artificial Intelligence Review*, 56(6):5545–5589, 2023.
- [67] Kai Yi, Bingxin Zhou, Yiqing Shen, Pietro Liò, and Yuguang Wang. Graph denoising diffusion for inverse protein folding. *Advances in Neural Information Processing Systems*, 36, 2024.

- [68] Shuai Zhang, Yong Chen, Wenyu Zhang, and Ruijun Feng. A novel ensemble deep learning model with dynamic error correction and multi-objective ensemble pruning for time series forecasting. *Information Sciences*, 544:427–445, 2021.
- [69] Zuobai Zhang, Minghao Xu, Aurelie C Lozano, Vijil Chenthamarakshan, Payel Das, and Jian Tang. Pre-training protein encoder via siamese sequence-structure diffusion trajectory prediction. *Advances in Neural Information Processing Systems*, 36, 2024.
- [70] Zhiyuan Zhao, Xueying Ding, and B Aditya Prakash. Pinnsformer: A transformer-based framework for physics-informed neural networks. *arXiv preprint arXiv:2307.11833*, 2023.
- [71] Anthony Zhou, Cooper Lorsung, Amir Pouya Hemmasian, and Amir Barati Farimani. Strategies for pretraining neural operators. *arXiv preprint arXiv:2406.08473*, 2024.

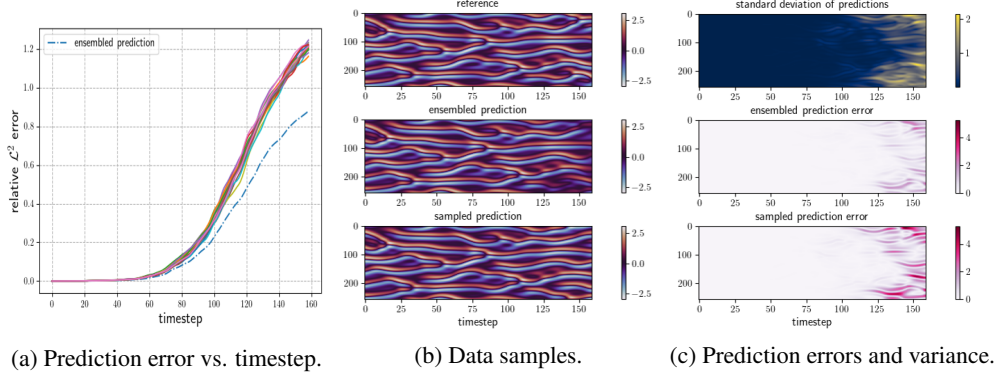


Figure 4: A comparison of prediction samples and their ensemble from PDE-Refiner.

A Experiment Details

A.1 PDE-Refiner

We choose to evaluate the ensembled prediction of PDE-Refiner on the Kuramoto-Sivashinsky 1D dataset. Model training and configuration follow the procedure specified in [40], with a U-Net architecture conditioned on the values of timestep size, spatial resolution, and viscosity value. To collect the model prediction results, we compute roll-out on all 128 trajectories of the test dataset for a duration of 159 timesteps. For each roll-out, we collect 16 prediction samples, denoted as $\{\tilde{u}^{(j)}\}_{j=1}^{16}$. Each sample $\tilde{u}^{(j)}$ has a shape $[B, T, D]$, where $B = 128$ is the number of simulation trajectories, $T = 159$ is the length of roll-out, and $D = 256$ is the spatial dimension. The ensembled prediction is computed as $\mu_u = \frac{1}{16} \sum_{j=0}^{16} \tilde{u}^{(j)}$. To compare the sampled predictions and their ensemble, we compute their relative \mathcal{L}^2 prediction error as follows.

$$e(t) = \frac{1}{B} \sum_{b=1}^B \frac{\|\hat{u}(b, t) - u(b, t)\|_2}{\|u(b, t)\|_2},$$

where \hat{u} is either a sampled prediction or the ensembled prediction, and $\|\cdot\|_2$ denotes the \mathcal{L}^2 -norm. A comparison of the prediction errors is shown in Fig. 4a. The error of ensembled prediction increases significantly more slowly over time than the error of any sampled prediction. Figures 4a and 4c provide visualization of prediction for a sampled data sequence. In particular, Fig. 4a shows the rollouts of a single model prediction sample (lower subplot), the ensembled prediction (central subplot) and the reference ground truth (upper subplot). Fig. 4c shows the point-wise absolute prediction error of a sampled rollout (lower subplot) and the ensembled rollout (mean: central subplot, variance: upper subplot), respectively. A quantitative comparison of model prediction errors is shown in the first row of Table 1, where the ensembled prediction has a lower prediction error than the average error of the 16 sampled rollouts at the final timestep. In fact, as shown in 4a, the ensembled prediction starts to outperform any sampled prediction after halfway of the simulation and maintains an increasing performance margin till the end of the simulation.

A.2 ACDM

To evaluate the effect of ensembled prediction on ACDM, we used a checkpoint trained to simulate the transonic cylinder flow for Mach numbers $Ma \in [0.53, 0.63] \cup [0.69, 0.90]$. At the inference stage, the model is tested on 6 simulation trajectories with Mach number ranging in $Ma \in [0.66, 0.68]$. Each trajectory has a length of 60 timesteps and is simulated via rollouts. Similar to the experiment with PDE-Refiner, we sampled 16 rollouts from each initial condition, resulting in a data shape of $[B, T, D, C]$, where $B = 6$ is the number of simulation trajectories, $T = 59$ is the length of roll-out, $D = 128 \times 64$ is the spatial dimension, and $C = 5$ is the number of data channels (horizontal velocity, vertical velocity, pressure, temperature, and Mach number). The sampled predictions and their ensemble (computed as the mean of all 16 samples) are evaluated with relative \mathcal{L}^2 prediction

error as follows.

$$e(t) = \frac{1}{B \cdot D \cdot C} \sum_{b=1}^B \sum_{d=1}^D \sum_{c=1}^C \frac{\|\hat{u}(b, t, d, c) - u(b, t, d, c)\|_2}{\|u(b, t, d, c)\|_2}, \quad (6)$$

where \hat{u} is denotes a sampled prediction or the ensembled prediction. As shown in Fig. 5a, the error of ensembled prediction is lower than any sampled prediction at the final timestep and for most parts of the rollouts. A visualization of data samples, point-wise prediction error and ensemble variance is provided in Fig. 5b. To visualize the uncertainty of model predictions, we show in Fig. 5c a time sequence of ensembled prediction and its uncertain (defined as the range spanned by the minimum and the maximum predictions), evaluated at the center of the 2D domain. A quantitative comparison of prediction accuracy with and without ensemble is shown in the second row of Table 1, where ensembled prediction is shown to yield a lower prediction error than the mean prediction error of all 16 samples by the end of the simulation rollout.

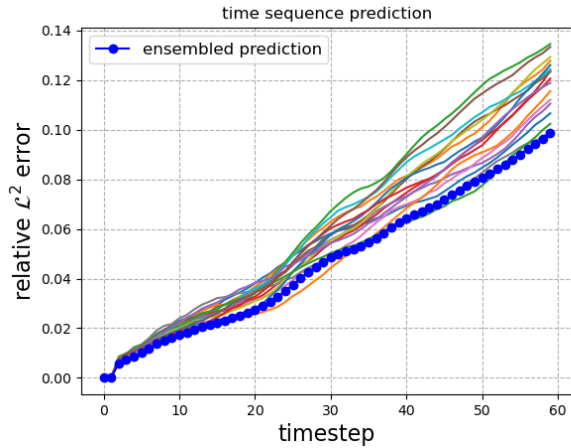
A.3 PI-DFS

Our numerical experiments are conducted to examine the impact of ensembled prediction on the performance of the PI-DFS model, including impacts on the relative \mathcal{L}^2 prediction error, the residual loss and statistical metrics such as the kinetic energy spectrum and vorticity distribution. The task of reconstructing high-fidelity vorticity data from low-fidelity inputs was carried out on a test dataset of the shape $[B, T, D]$, where $B = 4$ corresponds to four time sequences of turbulent flow vorticity in a 2D domain simulated by a numerical solver solving a Navier-Stokes equation, $T = 318$ is the number of timesteps of each time sequence, and $D = 256 \times 256$ specifies the size of the 2D domain. Similar to the experiments with PDE-Refiner and ACDM, given an input of low-fidelity vorticity data sampled from the test dataset, we generate 16 outputs from the PI-DFS model, and then compute their mean as the ensembled prediction of the high-fidelity vorticity data. The relative \mathcal{L}^2 loss and the relative residual loss (denoted as $e(t)$ and $r(t)$, respectively) are defined as follows.

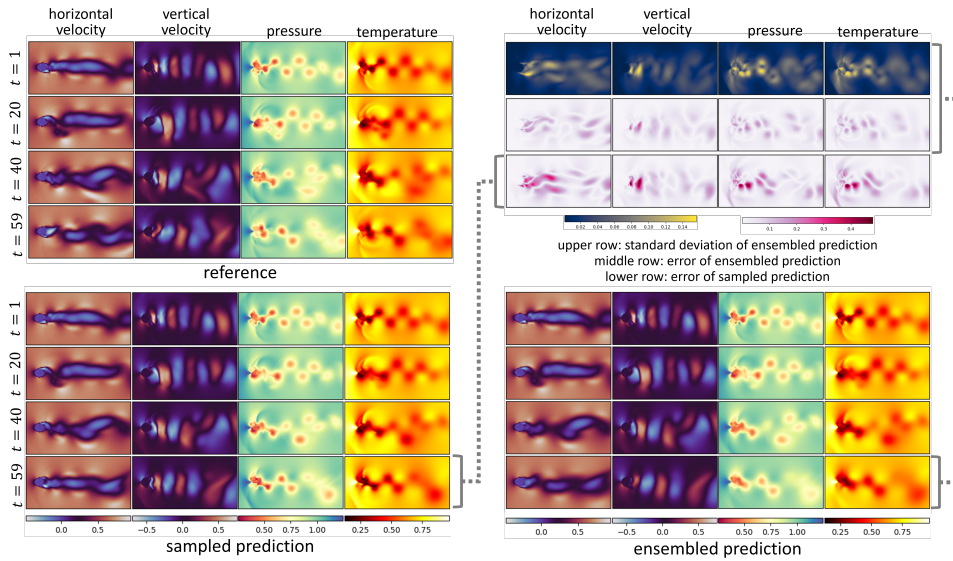
$$e(b, t) = \frac{\|\hat{\omega}(b, t) - \omega(b, t)\|_2}{\|\omega(b, t)\|_2}, \quad r(b, t) = \frac{1}{D} \sum_{d=1}^D \frac{|G(\hat{\omega}_d)|^2}{\|\omega\|_2^2},$$

where ω , $\hat{\omega}$ denote the ground truth and the predicted vorticities of the turbulent flow, respectively. $G(\cdot)$ denotes a differential operator defined by the Navier-Stokes equation, e.g., $G(u, du/dt, \partial u/\partial \xi_1, \dots, \partial^2 u/\partial \xi_1 \partial \xi_2, \dots; Re) = 0$, where u is the velocity vector, ξ_i is the spatial coordinate of the i -th direction, and Re is the Reynolds number.

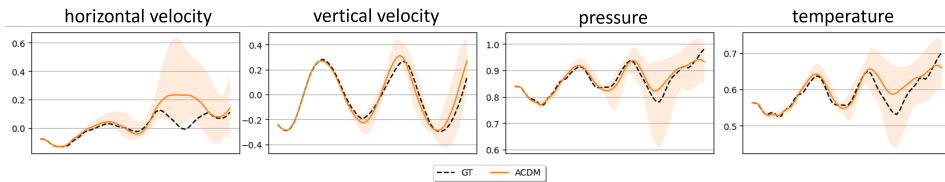
Figure 6 shows the relative \mathcal{L}^2 loss and the relative residual loss of the PI-DFS model on two simulation trajectories sampled from the test dataset. In terms of \mathcal{L}^2 loss, the variation between different prediction samples is smaller than the error variation of PDE-Refiner and ACDM. The ensembled prediction yields a marginal reduction in the relative \mathcal{L}^2 loss. However, the residual losses from different prediction samples show a larger variation. Unlike the cases of the other two models, ensembled prediction with PI-DFS does not always have a residual loss lower than any sampled prediction. Nevertheless, ensemble still gains a significant decrease in residual loss from the mean residual loss of all prediction samples, as shown in the third row of Table 1. For a visualization of data samples used in the numerical experiment with PI-DFS, Figure 8 shows the qualitative results of high-fidelity data reconstruction from a single prediction sample and from the ensemble of all prediction samples. Similar outcomes are observed in the visualization of the data samples (Columns 3 and 4, upper subfigure) and their point-wise absolute prediction errors (Columns 1 and 2, lower subfigure), whereas a more conspicuous difference can be observed in the point-wise absolute value of the PDE residual (Columns 4 and 5, lower subfigure). A visualization of point-wise variance of the ensembled prediction is also provided in Fig. 8 (Column 1, lower subfigure), where it can be observed that a larger variance tends to appear in regions with higher vorticity. For a more comprehensive evaluation of ensembled prediction, we also compared the qualities of ensembled prediction and four samples prediction samples in a statistical sense using the metrics of kinetic energy spectrum and vorticity distribution, as shown in Fig. 7. In terms of vorticity distribution (Fig. 7a), ensembled prediction yields a highly similar result to these four samples. In terms of the kinetic energy spectrum each prediction, ensemble produces a marginally less accurate result than the four sampled predictions. As shown in Fig. 7b, the kinetic energy spectrum of the ensembled prediction deviates further from the reference ground truth compared with that of any prediction sample on



(a) Prediction error vs. timestep.



(b) Visualization of data samples.



(c) Visualization of prediction uncertainty at the center of the 2D domain.

Figure 5: A comparison of prediction samples and their ensemble from ACDM.

higher wave numbers. The high similarity between different prediction samples in Fig. 7 indicates that the PI-DFS has a high consistency in the statistical accuracy of its prediction. The marginal reduction of accuracy in the energy spectrum of ensembled prediction is possibly a results losing some higher frequency spatial patterns due to the mean operation to obtain the ensembled prediction.

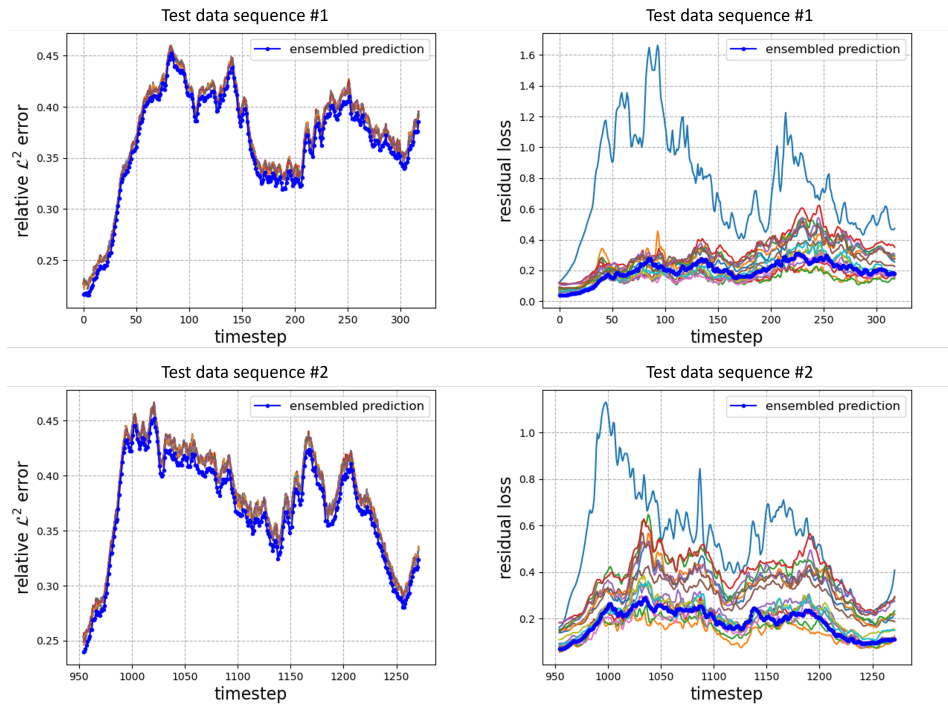
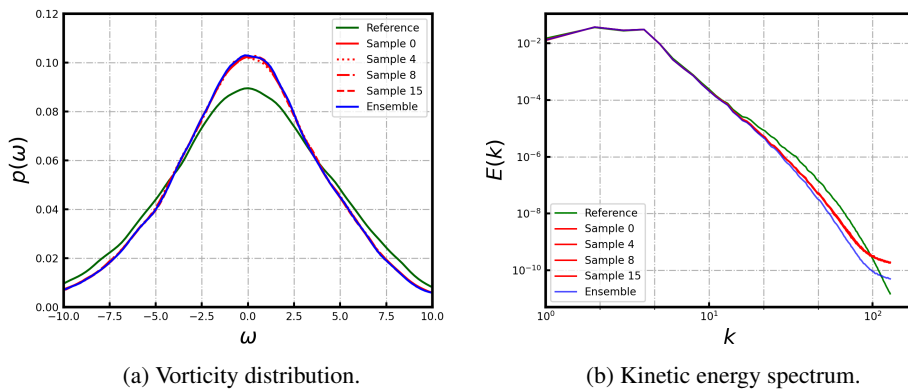


Figure 6: Prediction errors of model output samples and their ensemble on simulation trajectories from test data.



(a) Vorticity distribution.

(b) Kinetic energy spectrum.

Figure 7: A comparison of model prediction samples and ensemble using statistical metrics.

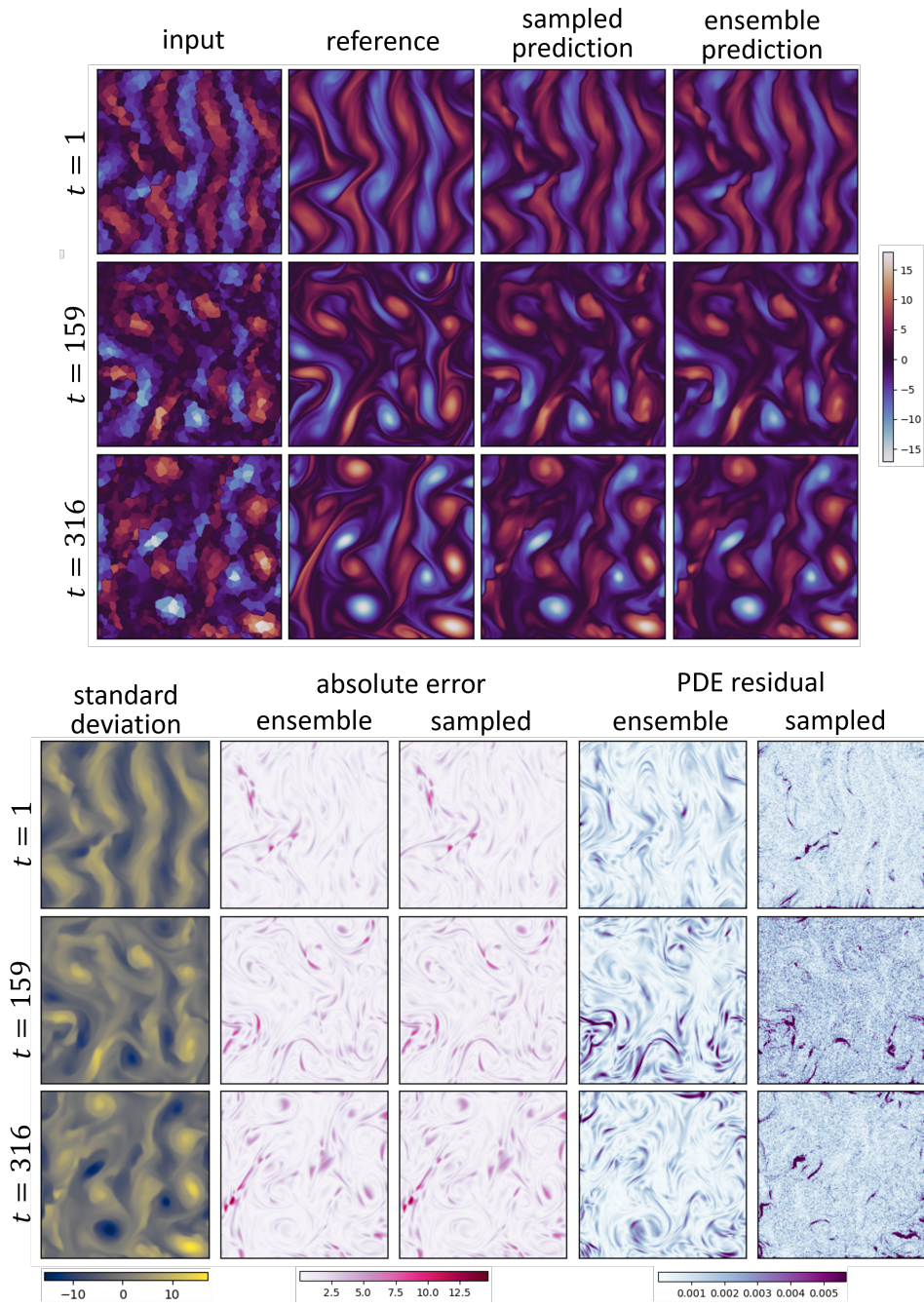


Figure 8: A comparison of prediction samples and their ensemble from PI-DFS.